

## MODELLING SHELL-SIDE CRUDE OIL FOULING IN SHELL-AND-TUBE HEAT EXCHANGERS

E. Diaz-Bejarano and F. Coletti

Hexxcell Ltd., Imperial College Incubator, Bessemer Building Level 2, Imperial College London, London SW7 2AZ, UK,  
[f.coletti@hexxcell.com](mailto:f.coletti@hexxcell.com)

### ABSTRACT

Crude oil fouling is a challenging, longstanding and costly problem for the oil industry. Very recently, mathematical models that are able to capture and predict fouling trends in crude shell-and-tube heat exchangers have emerged. One such example is the advanced model that powers Hexxcell Studio™ (Hexxcell Ltd., 2015). While the focus has been on fouling inside the tubes, fouling on the shell-side has generally been neglected because of the difficulties in modelling such complex geometries. However, in some instances fouling deposition on the shell-side plays a non-negligible role. Not only it impairs heat transfer but it also affects the hydraulics by increasing pressure drops and modifying flow paths.

This paper illustrates a new feature of Hexxcell Studio™ that allows capturing fouling on the shell-side of shell-and-tube heat exchangers. Simulation of an industrial exchanger shows the interaction between fouling growth inside and outside of the tubes and unveils the impact of fouling on shell-side flow patterns, heat transfer coefficient and pressure drops. It is also shown that if fouling on the shell-side is neglected, field data may be misinterpreted leading to wrong conclusions about the thermal and hydraulic performance of the heat exchanger.

### INTRODUCTION

Crude oil fouling in refinery preheat trains is a complex, costly and disruptive problem that has been affecting the refining industry for decades. In recent years, significant progress has been made in the fundamental understanding of the processes leading to fouling (Macchietto et al. 2011; Coletti and Hewitt 2015; Macchietto 2015) and in the fouling management strategies in industrial practice, involving the regular cleaning of key heat exchangers and/or the use of anti-foulants. However, there is still a significant room for improvement, particularly with regards to the design and condition monitoring of heat exchangers. Following a number of critiques of the fouling factor bases approach to heat exchanger design (Somerscales 1990; Chenoweth 1997), a significant effort has been made to develop alternative tools that allow capturing, predicting, managing and, ultimately, mitigating fouling.

Based on experimental measurements, various correlations that describe the thermal resistance given by

fouling as a function of process conditions and time have been proposed (Crittenden and Kolaczkowski 1987; Epstein 1994; Polley et al. 2002a; Nasr and Givi 2006)). Mathematical models that use such equations (Yeap et al. 2004; Ishiyama et al. 2010; Coletti et al. 2010) have been developed with the aim of improving existing design and monitoring software tools. One limitation of these models is that they consider deposition of fouling only on the tube-side. Thus their applicability is restricted to cases in which shell-side fouling is negligible.

Traditional design practice recommends allocating the fluid with the highest fouling propensity to the tube-side to allow easier and more effective cleaning. However, the shell-side fluid may also be prone to fouling, particularly with heavy fractions from the atmospheric or the vacuum distillation unit. An example of heavily fouled shell-side is shown in Fig. 1. In some cases not only shell-side fouling occurs but it can be the dominant resistance to heat transfer. In such cases, neglecting the thermal and hydraulic effects of shell-side deposition may lead to gross errors in the analysis of plant data. The above mentioned correlations relate fouling rates to tube side conditions. As a result, when shell-side fouling is relevant, the relationship between fouling rate and tube side operating conditions are not captured correctly, and thermal and hydraulic performance of the exchanger cannot be predicted correctly.



Fig. 1 Photo of shell-side fouling of refinery heat exchanger (Coletti et al. 2015). Reproduced with permission (Copyright 2015 Elsevier).

Given its complex geometry, it is not easy to calculate thermal and hydraulic performance on the shell-side. Tinker (1958) proposed a method based on a 'fluid flow fraction' concept whereby the effect of hydraulic resistances and dimensions for the different flow routes through the exchanger are taken into account (Fig. 2) thus the heat transfer coefficient and pressure drops are calculated as a function of geometrical parameters (baffle cut, baffle spacing, pitch angle and length etc.) and clearances (bundle-to-shell, shell-to-baffle and tube-to-baffle).

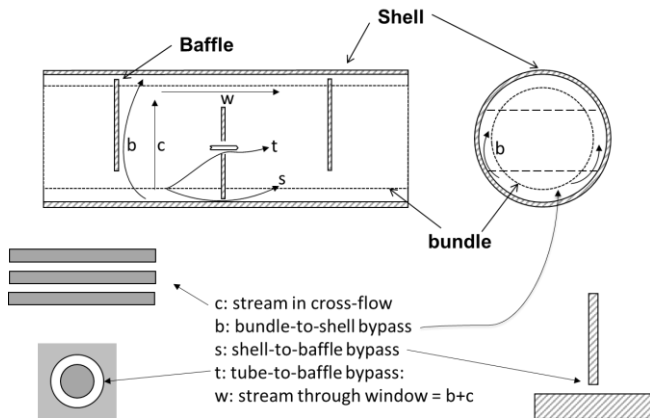


Fig. 2 Shell-side flow streams.

Following the approach by Tinker (1958), the Bell-Delaware (Bell 1963; Taborek 2008) and the Flow Stream Analysis (Hewitt, 2008) methods have been developed and are widely used in industry to calculate the thermal and hydraulic performance of the shell-side in clean conditions. However, all the methods mentioned above do not take into account the effects of fouling build-up. Indeed fouling affects the thermal and hydraulic performance of the shell-side in two areas:

1. The outer surface of the tubes (Fig 1). As a result of the build-up on this surface heat transfer with the inner side of the tube is impaired. Moreover, the reduction of the area available to the fluid flow increases the velocities in cross-flow increasing both convective heat transfer coefficient and pressure drops.
2. The shell clearances (bundle-to-shell, shell-to-baffle and tube-to-baffle). While the heat exchanger is clean, the flow fractions are determined by the geometrical clearances. As fouling builds up, these become occluded and the resistance to flow in the bypasses increase. As a result, the portion of cross-flow – and with it the thermal and hydraulic performance of the exchanger – changes over time.

In his original paper, Tinker (1958) already included some considerations on the effects of fouling on the clearances. He noted that baffle holes are likely to become completely plugged over an unspecified amount of time whilst other clearances may reduce to a certain percentage of the original clean geometry. He considered the case in which 80% of the flow passages have been restricted from the clean value. He noted that the increase in pressure drop as a result of this restriction was equivalent to increasing the flowrate by 25% in clean conditions. He suggested to use a multiplier in the

fluid fractions to adjust accordingly. Whilst this approach provides a way of determining fouled pressure drops, it heavily relies on the experience of the designer and does not take into account any dependence of fouling deposition on process conditions. As a result it cannot be used to find designs that minimize fouling.

Whilst to the authors' knowledge there are no models that consider both effects described above, some limited attempts exist describing shell-side fouling. Clarke and Nicolas (2000) presented a CFD model for an entire shell-side of a heat exchanger where the fraction occupied by the tubes is accounted for as a time-varying porosity. Fouling, predicted using the threshold model by Ebert and Panchal (1995), was used to gradually reduce porosity inside the shell. Significant limitations of this work are that calculated flow patterns were not realistic and, more importantly, its interactions between tube and shell-side were ignored. Vessakosol and Charoensuk (2010) studied the heat transfer and flow patterns around a tube in cross-flow (assumed to be laminar and steady-state) with fouling. The fouling layer was modelled as an annulus with constant thermal properties and various deposit conductivities and shapes of the fouling layer were investigated but the dynamics of deposition was neglected. Whilst these studies provide some insights into shell-side fouling, they require several difficult to measure parameters and are difficult to validate.

In this paper a new feature available in Hexxcell Studio™ (Hexxcell Ltd., 2015) is illustrated which allows capturing fouling on the shell-side of refinery heat exchangers. A case study is used to demonstrate the importance of considering shell-side fouling in order to correctly predict the thermo-hydraulic performance of a refinery shell-and-tube heat exchanger. Finally, one of the benefits of this new capability, namely the ability to discriminate between shell-side and tube-side fouling contributions to the overall heat transfer resistance is also discussed.

## APPROACH

The model for shell-and-tube heat exchangers undergoing fouling in Hexxcell Studio™ (Hexxcell Ltd. 2015) is extended to consider shell-side fouling. The model, based on that by Coletti and Macchietto (2011), is dynamic, distributed and captures tube-side fouling as a function of local conditions in each pass. The Coletti and Macchietto (2011) model comprises 4 spatial domains: shell-side flow ( $\Omega_s$ ), tube wall ( $\Omega_w$ ), tube-side fouling layer ( $\Omega_{L,t}$ ), and tube-side flow ( $\Omega_t$ ). A new fifth domain is introduced here to represent a fouling layer building up on the outer surface of the tubes. The new configuration, including the shell-side fouling domain ( $\Omega_{L,s}$ ), is shown in Fig 3. Other extensions include the use of Flow Stream Analysis to calculate shell-side pressure drops as well as the inclusion of the hydraulic effects of headers and nozzles (Sinnott 1999; Henry 2008). The following sections describe the models used to capture fouling on the outer surface of the tubes and on the clearances.

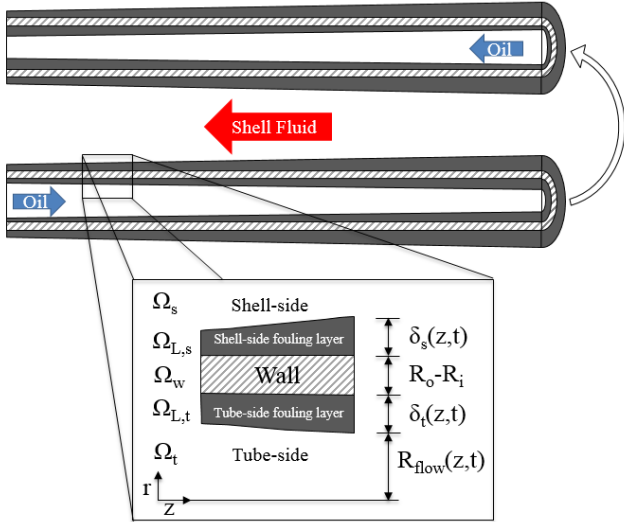


Fig. 3 Schematic representation of a two pass heat exchanger with inner and outer tube fouling.

### Outer tube fouling model

The deposit layer model by Coletti and Macchietto (2011), originally derived to simulate inside-tube fouling, is distributed over the axial and radial direction in each pass. The growth dynamics of the fouling layer was described with the use of a moving boundary problem where the boundary was moving inwards from the surface of the tube. Here, the original model is generalized to enable simulation of both inside and outside tube fouling. The heat balance in the deposit layer is:

$$\delta_n^2 \rho_L C_{p,L} \frac{\partial T_{L,n}}{\partial t} = \frac{\partial \lambda_{L,n}}{\partial \tilde{r}} \frac{\partial T_{L,n}}{\partial \tilde{r}} - \frac{\lambda_{L,n} \delta_n}{R_i - \tilde{r} \delta_n} \frac{\partial T_{L,n}}{\partial \tilde{r}} + \lambda_{L,n} \frac{\partial^2 T_{L,n}}{\partial \tilde{r}^2} \quad (1)$$

Quantities are defined in the nomenclature. The local thermal-conductivity ( $\lambda_{L,n}$ ) of the layer varies over time and as function of local temperature due to ageing. The time variation of the “youth” variable used to describe ageing (i.e. the changes in local thermal-conductivity of the fouling layer), is given by:

$$\frac{\partial y_n}{\partial t} = (1 - \tilde{r}) \left[ -A_a \exp\left(-\frac{E_a}{R_s T_L}\right) y \right] \quad (2)$$

The dimensionless radial coordinate ( $\tilde{r}$ ) is defined as:

$$\tilde{r} = \frac{r - R}{R_{flow}(t, z) - R} \quad (3)$$

where  $r$  is the dimensional radial coordinate,  $R$  is the radius corresponding to the interface between tube wall and fouling layer, and  $R_{flow}$  is the radius corresponding to the interface between fouling layer and fluid, which varies as fouling builds up. The difference between inside and outside fouling

relies on the definition of the reference radii (inner radius for inside tube fouling,  $R_i$ ; outer radius for outside tube fouling,  $R_o$ ). In both cases,  $\tilde{r} = 1$  corresponds to the surface of the fouling layer (i.e the interface with the fluid flow), and  $\tilde{r} = 0$  corresponds to the wall surface. The boundary conditions are defined as indicated in the reference papers, providing continuity to the heat flux and temperature radial profiles.

### Fouling rate

The deposition rate, in terms of rate of change of deposit thickness, is calculated using the threshold fouling model (Panchal *et al.* 1997), written in terms of fouling layer thickness, for both tube-side and shell-side:

$$\frac{d\delta}{dt} = \lambda_0 \alpha \text{Re}^{-0.66} \text{Pr}^{-0.33} \exp\left(-\frac{E_f}{R_g T_{film}}\right) - \lambda_0 \gamma \tau \quad (4)$$

The deposition rate in Eq. (4) is a function of the local conditions along the heat exchanger on each side and for each pass. On the tube-side,  $\tau$  is the wall shear stress, as originally proposed by Ebert and Panchal (1995) thus friction is considered to be dominating the suppression/removal of the deposit.

The potential application of the threshold fouling model to the shell-side and other systems (i.e. tube inserts) was discussed by Polley *et al.* (2002b). The pressure drop in the shell-side is a combination of skin friction and drag. The authors argued that only skin friction is responsible for the removal term, and noted that it was not possible to calculate shear stress in the shell-side because of its complex geometry. Instead, they proposed to replace  $\tau$  with a function of Reynolds number ( $\text{Re}^{0.8}$ ).

The total loss of energy for cross-flow through tube banks has been measured experimentally as a function of Reynolds number, leading to correlations for the drag coefficient for various bundle configurations (as functions of  $\text{Re}$ ) (Zukauskas and Ulinskas 2008). For the shell-side, the wall shear stress in Eq. (4) is substituted with the total force per unit of tube area based on such correlations. Since this quantity includes drag and skin friction, it is assumed here that both drag (turbulence) and friction affect removal/suppression.

Based on the above discussion, it should be noted that it is not possible to use on the shell-side the same values of the fouling parameters estimated on the tube-side. Instead, shell-side fouling parameters need to be estimated independently.

### Occlusion of clearances

As mentioned in the introduction, traditional shell-side calculations such as the Bell-Delaware and Flow Stream Analysis consider the effect of leakage through clearances on heat transfer coefficients and pressure drops only in clean conditions. Here, the progressive occlusion of the clearances produced by fouling (schematically shown in Fig. 4) is considered. Fouling build-up on the inner surface of the shell is also considered. Fouling deposition on the inner shell surface does not affect the thermal model directly (i.e.

heat exchange between fluids or between shell and the environment) but only the various clearances (bundle-to-shell and baffle-to-shell), thus flow redistribution and (indirectly) on the shell-side heat transfer coefficient and pressure drop.

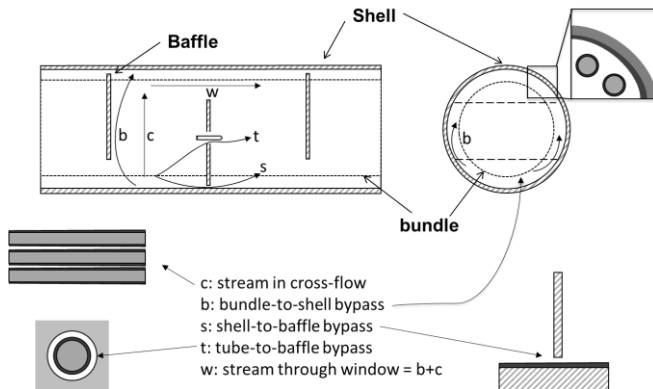


Fig. 4 Flow streams in shell-side and schematic representation of occlusion of clearances due to fouling.

The main assumptions are:

- i) Clearances are uniform throughout the length of the heat exchanger, that is, occlusions are calculated for an average deposit thickness on the shell-side.
- ii) Local flow patterns near the clearances are neglected.
- iii) Deposit thickness on the inner surface of the shell is equal to the average thickness on the outer tube surface.

## CASE STUDY

The same double-shell refinery heat exchanger with 4 tube pass (Fig. 5) previously studied by Coletti and Macchietto (2011) is considered. This unit was reported by plant personnel not to have any significant fouling on the shell-side, by visual inspection during shut down. Coletti and Macchietto (2011) reported that their model with only tube-side fouling could successfully capture the fouling behavior using historical plant data and accurately predict the performance of the unit over a year of operation.

## RESULTS

### Interpretation of Refinery Data

The inclusion of a shell-side fouling model introduces new degrees of freedom in the model. The effect of fouling on the thermo-hydraulic performance of the exchanger can now be explained by a combination of deposit thickness and conductivity on both tube and shell-side. Due to the thermal coupling between shell and tube-sides, there are many possible solutions to the problem, that is, the same thermal performance may be achieved by allocating the various proportions of the overall thermal resistance to the tube to the shell. On the other hand, shifting fouling resistance from one side to the other implies shifting part of the fouling layer thickness, which affects the system hydraulics, i.e. pressure drops. Here, the use of pressure drop measurements to decouple tube and shell-side fouling is explored.

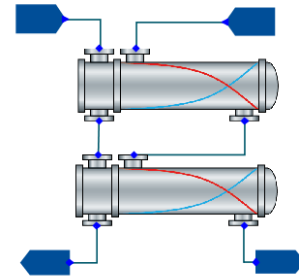


Fig. 5 Double-shell heat exchanger as shown in the user interface in Hexxcell Studio™.

From a modelling point of view, the presence of new degrees of freedom implies a greater number of fouling and conductivity parameters that must be fitted in order to capture the growth of the deposit and its thermal resistance. Here, rather than using  $\Delta P$  measurements (which were unavailable for this exchanger) to estimate both shell and tube fouling parameters, a proportionality between shell and tube fouling rates is assumed.

$$\alpha_s = K\alpha_t; \gamma_s = K\gamma_t \quad (5)$$

where  $K$  is a proportionality constant that is fixed a priori. On both shell and tube side, the deposition rate is given by Eq. 4. The parameter estimation method detailed in Coletti and Macchietto (2011) is applied to estimate the tube-side fouling parameters ( $\alpha$ ,  $E_t$ ,  $\gamma$ ) based on outlet temperatures of tube and shell-side: the first 60 days of operation after cleaning are used to estimate the fouling parameters; then all parameters are fixed, and the model is used to predict fouling behavior until the end of the operation period (1 year). This method is applicable in cases where: a) shell-side fouling is negligible; and b) the deposit is composed of organic material, for which the proposed ageing model (Eq. (2)) can be assumed to adequately represent the evolution of the deposit conductivity. Here, with the extra degrees of freedom eliminated by fixing the proportionality constant  $K$ , the method can still be applied. The same type of foulant, organic matter undergoing ageing, is assumed for shell and tube-side (for details on ageing model see Coletti and Macchietto, 2011). Multiple scenarios were considered with  $K$  varying from 0 (no shell-side fouling) to 1 (same parameters) and with  $K = \infty$  (no tube-side fouling). Finally, predicted thermal and hydraulic performance is compared for the various cases.

The parameter estimation results are shown in Table 1. Figure 6 shows the residuals of the simulated outlet temperatures vs. plant measurements for the different scenarios, calculated according to Eq. (6).

$$Error(\%) = 100 \frac{measured - predicted}{measured} \quad (6)$$

In all cases, the estimation was carried out successfully, producing a good fitting of the measurements during the first 60 days.

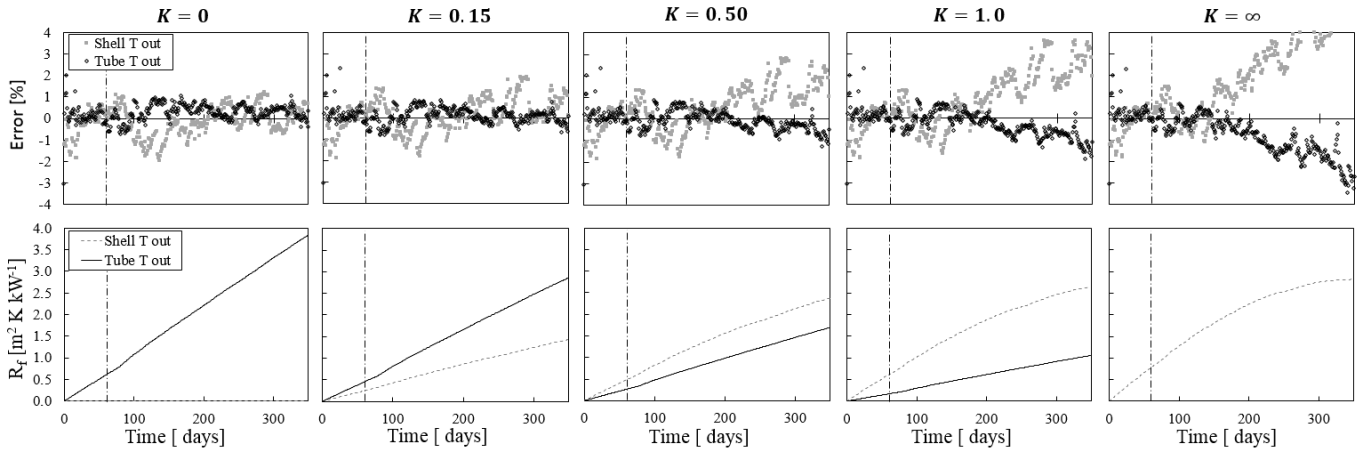


Fig. 6 Relative error and fouling resistance referred to the outer tube area for the various ratios of shell to tube fouling rate. The dashed-dot line indicates the end of the estimation period.

This indicates that a number of combinations of parameters exist that explain the thermal performance of the unit. However, not all combinations of parameters are able to extrapolate and the outlet temperatures for the rest of the year with the same level of accuracy. For small values of  $K$ , the outlet temperatures are within  $\pm 1\%$  for the tube and  $\pm 2\%$  for the shell-side of the measured outlet temperature. For larger values of  $K$ , a clear deviation is observed after 200 days. This seems to indicate that the set of parameters that best represents the actual behaviour is for fouling only on the tube-side. This correlates well with plant observations. However, this could also be related to inaccuracy in the assumptions, such as the proportionality between tube and shell parameters (assumed the same for both deposition and removal constants) or the fouling rate model assumed for the shell-side. Fig 6 also shows the average fouling resistance for shell and tube-sides. Whilst the proportion of the thermal resistance is gradually shifted from tube to shell with increasing values of  $K$ , the overall thermal performance is similar in all cases. It should be noted that, when the same values of the fouling parameters are used on both tube and shell side (i.e.  $K=1$ ) a much faster deposition rate on the shell-side is calculated, thus confirming that parameter portability between the two sides is not possible.

Table 1. Tube-side fouling parameters for various values of the proportionality constant  $K$ .

$K$	$\alpha$ ( $m^2 K J^{-1}$ )	$E_f$ (J/mol)	$\gamma$ ( $m^4 K J^{-1} N^{-1}$ )
0	0.00165	28491	$9.28 \cdot 10^{-13}$
0.15	0.00122	28906	$9.13 \cdot 10^{-13}$
0.50	0.00075	29016	$8.94 \cdot 10^{-13}$
1	0.00052	29371	$8.21 \cdot 10^{-13}$
$\infty$	0.00056	28564	$7.20 \cdot 10^{-13}$

The results show that the thermal performance of the heat exchanger can be explained by allocating in different proportions the heat transfer resistance between the shell and tube side, the hydraulic behaviour is not. Fig. 7 shows the pressure drop on the tube-side for the different values of  $K$ . As the portion of the fouling resistance is attributed to shell-side increases, the pressure drop varies dramatically.

This indicates that pressure drop measurements, if available, could be used to identify the location of fouling. Moreover, Fig 7 shows that pressure drops become increasingly sensitive to fouling over time. This implies that pressure drop in the early stages be useful only if very accurate sensors are used. The high pressure drops calculated for low values of  $K$  are consistent with reported industrial values (Mozdianfard and Behranvand, 2015).

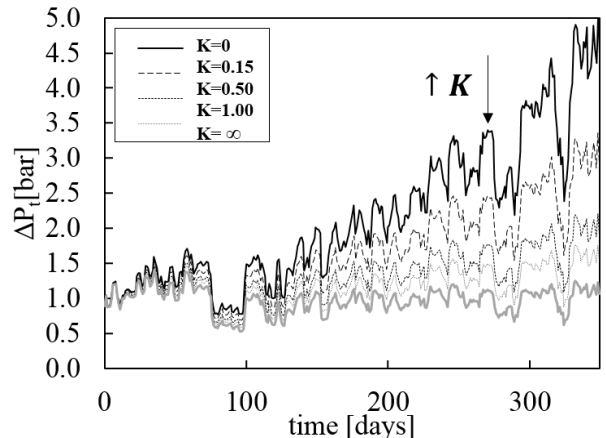


Fig. 7 Pressure drop on the tube-side for different shell to tube fouling rate ratios

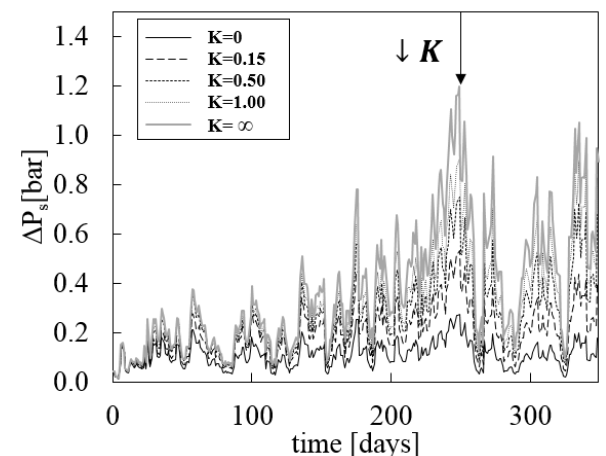


Fig. 8 Pressure drop on the shell-side for different shell to tube fouling rate ratios.

Fig. 8 shows the shell-side pressure drop. In this case, the pressure drop increases as the fouling proportion shifts from tube to shell (i.e. increasing  $K$ ). The major variation is observed between  $K = 0$  (no shell-side fouling) and  $K = 0.15$ . From Fig. 8 it can also be noticed that, as expected, the impact of fouling on the overall pressure drop is much lower than on the tube-side. As a result, pressure drop measurements on the shell-side would be less useful than tube-side ones to determine fouling layer thickness.

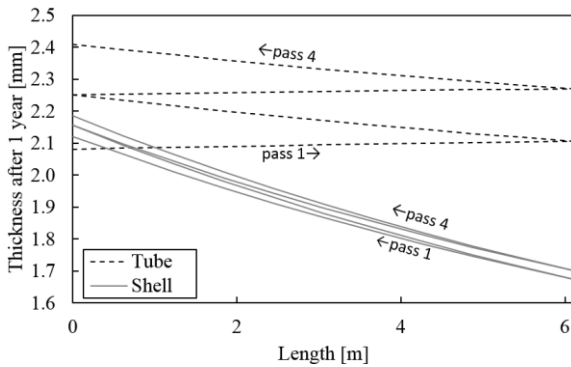


Fig. 9 Deposit thickness after 1 year of simulation for shell (continuous line) and tube (dashed line) in Shell A.

**Thermal-Hydraulic Impact of Shell-side Fouling**

In this section, the impact of the outer tube fouling on shell-side heat transfer coefficients and pressure drop is investigated in further detail for Shell A. For this purpose, fixed inlet conditions of temperature and flowrate and the fouling parameters obtained in the previous section for  $K = 0.15$  are considered (as an example of fouling occurring on both sides). The simulation is run for 1 year starting from clean conditions.

The growth of a fouling layer impacts heat transfer and pressure drop on both tube and shell side. This growth will be function of the local conditions. The thickness may vary significantly along the unit. Fig. 9 shows the deposit thickness on both tube and shell side for each pass after 1 year. The longitudinal variation of the deposit thickness is more relevant for the shell-side following the larger temperature gradient experienced by the fluid on this side of the exchanger.

One useful feature of the model is its ability to capture the effect of fouling on the shell-side clearances. Fig. 10 shows that the tube-to-baffle clearance becomes completely blocked after 77 days of operation. The rest of the clearances, except shell-to-bundle, are also reduced significantly (by 50-60% after 1 year). The shell-to-bundle clearance in this heat exchanger is unusually large, and therefore, in relative terms, fouling does not impact the flow significantly.

Model simulations also allow quantifying the variations in the flow fractions inside the shell-side due to the gradual occlusion produced by fouling (Fig. 11). In clean conditions, for this particular geometry and operating conditions, leakages account for 77% of the total flow. As fouling builds up, the flow distribution on the shell-side changes. In the early stages the tube-to-baffle clearance

becomes blocked and the corresponding leakage is diverted to the other flow paths. As the resistances for cross-flow and shell-to-baffle become important, the flow tends to go through the (as noted, unusually large) shell-to-bundle bypass area instead.

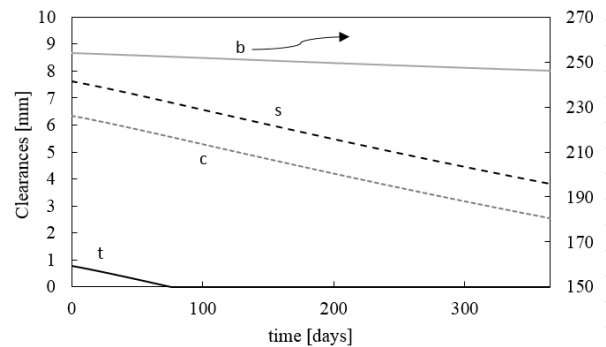


Fig. 10 Occlusion of clearances due to fouling in Shell A. Labels b, c, s, and t indicate flow streams (see Fig. 4).

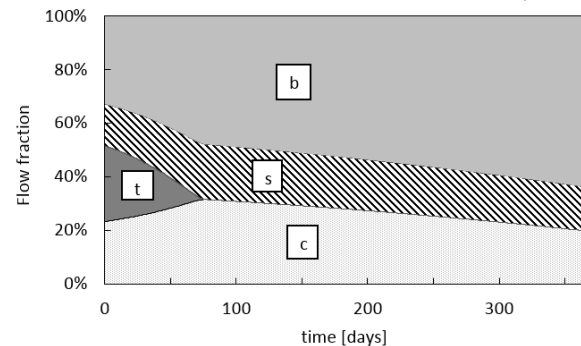


Fig. 11 Time evolution of flow fraction through shell-side paths due to fouling in Shell A. Labels b, c, s, and t indicate flow streams (see Fig. 4).

Shell-side fouling, as described here, has two main effects on the thermal performance of the heat exchanger: i) it decreases the overall heat transfer coefficient, hence reducing the heat transfer rate; ii) it increases the Reynolds number in crossflow, hence it enhances the convective heat transfer coefficient, and promotes suppression/removal mechanisms. In order to understand the importance of including the latter effect, the cases in which fouling affects the outer tube heat transfer with or without affecting the clearances are compared. Fig 12 shows the time evolution of the thickness in the first pass for tube-side and shell-side, considering and neglecting the impact of shell-side fouling on clearances. When the clearance occlusion is considered the space available for flow between tubes decreases leading to higher shear stress and drag forces, thus reduced fouling rate and thinner fouling layer.

Figure 13 shows the shell-side heat transfer coefficient over time considering and neglecting clearance occlusion. When no occlusion is considered, the coefficient slightly increases over time, due to the increase in temperature of the shell side fluid as fouling progresses (reduced heat transfer). When the effect of occlusion is considered, the increase in heat transfer coefficient is much more significant. The gradual increase in Reynolds number, produced by the progressive restriction of the flow area and the increased

cross-flow fraction generated by the blockage of the clearances, partly offsets the decrease in heat transfer due to fouling deposition. Two distinct slopes can be identified in this case, which correspond to the period before and after complete blockage of tube-to-baffle clearance.

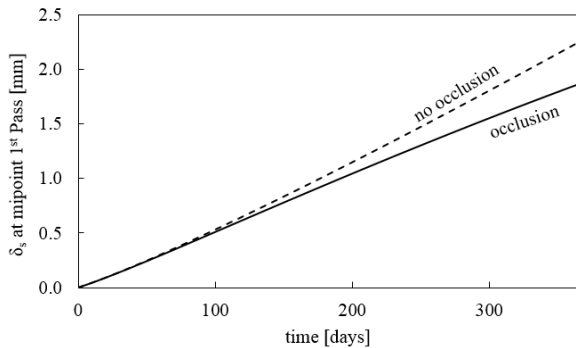


Fig. 12 Outside-tube thickness at midpoint of 1<sup>st</sup> Pass (Shell A) over time.

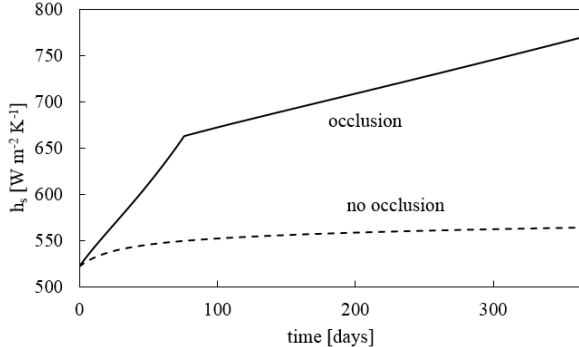


Fig. 13 Shell-side heat transfer coefficient over time with and without occlusion of clearances.

In terms of the hydraulic performance, the occlusion of clearances leads to increased pressure drop over time (Fig. 14). If occlusion of clearances is considered, the pressure drop is doubled after a year of operation. Nevertheless, sensitivity of pressure drop on fouling is not as significant as in the tube-side, as a result of the availability of multiple flow paths for flow redistribution. It should be noted that in this case, the large bundle-to-shell bypass helps maintaining hydraulic performance as fouling builds up.

## CONCLUSIONS

In this paper, a model for shell-side fouling in refinery heat exchangers has been presented. To the authors' knowledge this is the first time that the effects of shell-side fouling build-up on heat exchange, shell-side heat transfer coefficient and pressure drop are described taking into account simultaneously deposition on the outer tube surfaces and the progressive blockage of the shell-side clearances. The model, implemented in Hexxcell Studio™, is dynamic and distributed and considers the interaction of tube-side and shell-side local fouling rates.

Based on an industrial example, it has been shown that the observed *thermal* performance based on plant data can be captured with similar accuracy both considering or neglecting shell-side fouling. These results show the potential misinterpretation of plant data if shell-side fouling

is completely neglected. This is particularly important when trying to fit fouling models to measurements of operating conditions. Wrong relationships could be captured, leading to: a) models that fail to predict fouling behavior if those conditions were to change in the future; and b) wrong mitigation decisions based on, for instance, heat exchanger design using the threshold concept or similar on the tube-side.

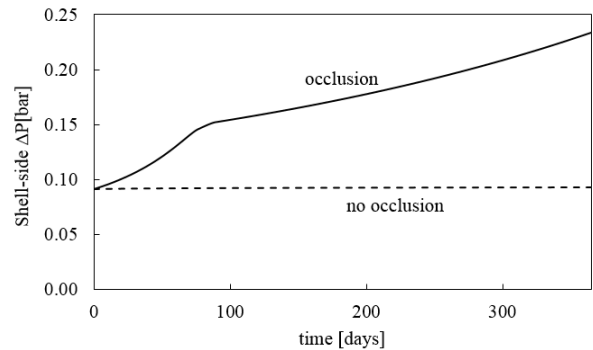


Fig. 14 Shell-side pressure drop over time with and without occlusion of clearances.

Provided that the conductivity of the deposits is reasonably known (e.g. the main fouling mechanism is organic deposition), pressure drop measurements could be potentially used to decouple shell and tube-side fouling. The study has shown that pressure drop on the tube-side seems to be more sensitive to fouling than that on the shell-side. It is therefore recommended that hydraulic performance on the tube-side should be monitored.

The case study shown illustrates the need for models that consider both thermal and hydraulic impacts of fouling. This feature enables taking full advantage of the information provided by primary pressure drop measurements available, and using them in the estimation of key parameters. Finally, consideration of occlusion of clearances due to fouling has been shown to affect fouling rate, heat transfer coefficient, and pressure drop on the shell-side.

## NOMENCLATURE

$A_a$	Ageing activation energy, 1/s
$C_p$	Specific heat capacity, J/kg
$E_a$	Ageing activation energy, J/mol
$E_f$	Fouling activation energy, J/mol
$h$	Heat transfer coefficient, $W/m^2 K$
$K$	Proportionality constant, dimensionless
$n$	Pass number
$Pr$	Prandtl number, $C_p\mu/\lambda$ , dimensionless
$R$	Radius, m
$R_{flow}$	Radius at the fouling layer-fluid interphase, m
$R_g$	Ideal gas constant, 8.314 J/molK
$r$	Radial coordinate, m
$\tilde{r}$	Dimensionless radial coordinate, dimensionless
$Re$	Reynolds number, dimensionless
$t$	Time, s
$T$	Temperature, K
$T_{film}$	Film Temperature, K
$y$	Deposit youth, -
$z$	Axial coordinate, m

$\alpha$	Deposition constant, $\text{m}^2 \text{K J}^{-1}$
$\gamma$	Suppression constant, $\text{m}^4 \text{K J}^{-1} \text{N}^{-1}$
$\delta$	Deposit thickness, m
$\Delta P$	Pressure drop, Pa
$\lambda$	Thermal-conductivity, W/mK
$\rho$	Density, $\text{kg/m}^3$
$\tau$	Shear stress, $\text{N/m}^2$

**Subscript**

0	initial
i	inner
L	layer
o	outer
s	shell
t	tube
w	wall

**REFERENCES**

- Bell, K.J., 1963. Final report of the cooperative research program on shell and tube heat exchangers. In *University of Delaware Engineering Experimental Station Bulletin No. 5*. Newark, Delaware.
- Chenoweth, J.M., 1997. The TEMA Standards fouling section: another look. In C. B. Panchal, ed. *Fouling Mitigation of Industrial Heat-Exchange Equipment*. New York: Begell House Inc.
- Clarke, R.H. and Nicolas, F., 2000. CFD Investigation of Maldistribution Effects on Crude-oil Fouling in Shell and Tube Exchangers. In *Second Int Conf on Petroleum and Gas Phase Behaviour and Fouling*. Copenhagen, Denmark.
- Coletti, F., Ishiyama, E.M., Paterson, W.R., Wilson, D.I. and Macchietto, S., 2010. Impact of Deposit Aging and Surface Roughness on Thermal Fouling : Distributed Model. *AIChE J*, 56(12), pp.3257–3273.
- Coletti, F., Joshi, H.M., Macchietto, S. and Hewitt, G.F., 2015. Introduction to Crude Oil Fouling. In F. Coletti and G. F. Hewitt, eds. *Crude Oil Fouling: Deposit Characterization, Measurements, and Modeling*. Boston, USA: Gulf Professional Publishing (Elsevier).
- Coletti, F. and Hewitt, G.F., 2015. *Crude Oil Fouling. Deposit Characterization, Measurements, and Modeling*. Boston, USA: Gulf Professional Publishing (Elsevier).
- Coletti, F. and Macchietto, S., 2011. A Dynamic, Distributed Model of Shell-and-Tube Heat Exchangers Undergoing Crude Oil Fouling. *Ind & Eng Chem Res*, 50(8), pp.4515–4533.
- Crittenden, B.D. and Kolaczkowski, S.T., 1987. Modelling Hydrocarbon Fouling. *Chem Eng Res & Des*, 65(2), pp.171–179.
- Ebert, W.A. and Panchal, C.B., 1995. Analysis of Exxon crude-oil slip stream coking data. In C. B. Panchal, ed. *Fouling Mitigation of Industrial Heat-Exchange Equipment*. San Luis Obispo, CA: Begell House, pp. 451–460.
- Epstein, N., 1994. A model of the initial chemical reaction fouling rate for flow within a heated tube, and its verification. In *10th Int Heat Transfer Conf*. Rugby, pp. 225–229.
- Henry, J.A.R., 2008. Headers, Nozzles, and Turnarounds. In G. F. Hewitt, ed. *Heat Exchanger Design Handbook*. Redding (USA): Begell House.
- Hewitt, G.F., 2008. Flow Stream Analysis Method for Segmentally Baffled Shell and Tube Heat Exchangers. In *Heat Exchanger Design Handbook*. Redding (USA): Begell House.
- Hexxcell Ltd., 2015. Hexxcell Studio. www.hexxcell.com.
- Ishiyama, E.M., Coletti, F., Macchietto, S., Paterson, W.R. and Wilson, D.I., 2010. Impact of Deposit Ageing on Thermal Fouling : Lumped Parameter Model. *AIChE J*, 56(2), pp.531–545.
- Macchietto, S., 2015. Energy Efficient Heat Exchange in Fouling Conditions: the UNIHEAT Project. In *Heat Exchanger Fouling and Cleaning XI*. Enfield (Ireland).
- Macchietto, S. et al., 2011. Fouling in Crude Oil Preheat Trains: A Systematic Solution to an Old Problem. *Heat Transf Eng*, 32(3-4), pp.197–215.
- Mozdianfar M. R. and Behranvand E., 2015, Fouling at post desalter and preflash drum heat exchangers of CDU preheat train, *Appl Therm Eng*, 89, pp. 783-794.
- Nasr, M.R.J. and Givi, M.M., 2006. Modeling of crude oil fouling in preheat exchangers of refinery distillation units. *Appl Therm Eng*, 26(14-15), pp.1572–1577.
- Panchal, C.B., Kuru, W.C., Liao, C.F., Ebert, W.A. and Palen, J.W., 1997. Threshold conditions for crude oil fouling. In T. R. Bott, ed. *Understanding Heat Exchanger Fouling and its Mitigation*. Lucca, Italy: Begell House, pp. 273–281.
- Polley, G.T., Wilson, D.I., Yeap, B.L. and Pugh, S.J., 2002a. Evaluation of laboratory crude oil threshold fouling data for application to refinery pre-heat trains. *Appl Therm Eng*, 22(7), pp.777–788.
- Polley, G.T., Wilson, D.I., Yeap, B.L. and Pugh, S.J., 2002b. Use of crude oil fouling threshold data in heat exchanger design. *Appl Therm Eng*, 22(7), pp.763–776.
- Sinnot, R.K., 1999. *Coulson and Richardson's Chemical Engineering; Vol 6, Chemical Engineering Design* 3rd ed., Oxford: Butterworth Heinemann.
- Somerscales, E.F.C., 1990. Fouling of heat transfer surfaces an historical review. *Heat Transf Eng*, 11(1), pp.19–36.
- Taborek, J., 2008. Calculation of Heat Transfer Coefficient and Pressure Drop. In G. F. Hewitt, ed. *Heat Exchanger Design Handbook*. Redding (USA): Begell House.
- Tinker, T., 1958. Shell-side characteristics of shell-and-tube heat exchangers. *Trans. ASME*, 80(1), pp.36–52.
- Vessakosol, P. and Charoensuk, J., 2010. Numerical analysis of heat transfer and flow field around cross-flow heat exchanger tube with fouling. *Appl Therm Eng*, 30(10), pp.1170–1178.
- Yeap, B.L. et al., 2004. Mitigation of crude oil refinery heat exchanger fouling through retrofits based on thermo-hydraulic fouling models. *Chem Eng Res & Des*, 82(A1), pp.53–71.
- Zukauskas, A. and Ulinskas, R., 2008. Banks of plain and finned tubes. In G. F. Hewitt, ed. *Heat Exchanger Design Handbook*. Redding (USA): Begell House.